Available online at www.sciencedirect.com
ScienceDirect
International Journal of Heat and Mass Transfer 51 (2008) 1818–1829
International Journal of HEAT and MASS TRANSFER
www.elsevier.com/locate/ijhmt

Numerical simulation and theoretical analysis of premixed low-velocity filtration combustion

Jun-Rui Shi [a,b,*], Mao-Zhao Xie [a], Hong Liu [a], Gang Li [c], Lei Zhou [a]

[a] School of Energy and Power Engineering, Dalian University of Technology, Dalian 116024, China
[b] Department of Power Engineering, Shenyang Institute of Engineering, Shenyang 110136, China
[c] Civil and Architecture Engineering College, Dalian University, Dalian 116622, China

Received 27 December 2006; received in revised form 25 June 2007
Available online 25 September 2007

Abstract

This paper investigates combustion wave characteristics of lean premixtures in a porous medium burner. Heat recuperation originated by the porous medium is examined by an one-dimensional numerical model. Attention is focused on the influences of solid properties, heat loss, equivalence ratio, etc., on the combustion wave speed and the maximum combustion temperature attained in the wave. Based on the flame sheet assumption a relationship between the combustion wave speed and the maximum combustion temperature is given. Then an approach from the laminar premixed flame theory is applied and the entire flame zone is divided into a pre-heating region and a reaction region, and treated separately. In this way, the second relationship between the two parameters is deduced. Thus a closed analytical solution for the combustion wave speed and the maximum combustion temperature is obtained. Over a wide range of working conditions, the numerical predictions and theoretical results show qualitative agreements with experimental data available from the literature. The results reveal that the mechanism of superadiabatic combustion is attributed to the overlapping of the thermal wave and combustion wave under certain conditions.

Keywords: Lean mixture; Low-velocity filtration combustion; Numerical simulation; Theoretical analysis

1. Introduction

The research of filtration combustion in porous media is drawing more and more attention in recent years: not only for its wide applications, ranging from hydrogen production, oil recovery, porous burner and heater, coal gasification, combustion of low-calorific fuels to diesel engines, but also for the good performance regarding emission products.

Filtration combustion in inert porous media covers a wide range and has been investigated extensively in the literature including experimental [1–4], analytical [5–7] and numerical studies [2,6,8]. Howell et al. [9] presented a detailed review of this subject. Recent advance and remaining questions in this area are summarized and reviewed by Kamal and Mohamad [10].

In order to realize steady combustion in inert porous media, the combustion wave has to be confined and held inside the combustor. In general, there are two design approaches commonly employed in porous combustion: stationary and transient systems. In the first system steady combustion can be achieved by controlling and holding the combustion wave at the interface between two porous media with different porosities or structures. However, this is difficult for a transient system since in this case combustion waves may move freely in the same or opposite directions as the flow of inlet mixtures. Thus, methods to confine and fix the combustion wave within a specific section of the combustor have to be developed and it is

* Corresponding author. Tel.: +86 411 84700067. Address: School of Energy and Power Engineering, Dalian University of Technology, Dalian 116024, China.
E-mail address: shijunrui2002@163.com (J.-R. Shi).

0017-9310/$ - see front matter © 2007 Elsevier Ltd. All rights reserved.
doi:10.1016/j.ijheatmasstransfer.2007.06.028

Nomenclature

A	pre-exponential factor
c	specific heat
d	average diameter of sphere diameter
E	activation energy
h_v	convective heat factor
Nu	Nusselt number
P	pressure
Pr	Prandtl number
Q	low heating value
R	universal gas constant
Re	Reynolds number
T	temperature
T_0	ambient temperature
u_g	gas velocity
u_t	thermal wave speed
u_w	combustion wave speed

Greek symbols

φ	equivalence ratio
ε	porosity
ρ	density
σ	Stephan–Boltzmann constant
λ	thermal conductivity
ω_i	reaction rate of ith species
β	heat loss factor

Subscripts

g	gas
s	solid

imperative for both theory and practical applications to clarify the mechanism of combustion wave propagation in porous media.

The low velocity regime (LVR) of filtration combustion, according to the classification suggested by Babkin [11], is of great importance in engineering applications and is characterized by an intense heat exchange between the solid and gas phases and a combustion wave velocity of about 0.1 mm/s. Zhdanok et al. [1] observed experimentally stable combustion waves (with a velocity less than the mixture velocities by a magnitude order of 3) co-current with the gas flow and the superadiabatic effect was confirmed by both experiments and a simplified mathematical analysis. They firstly revealed coupling between the thermal and combustion waves. It was shown that the temperature increase across the wave was a function of the adiabatic temperature T_{ad} of the given gas mixture and a "coincidence condition", namely the ratio between the combustion wave speed u_w and thermal wave speed u_t in the porous media:

$$\Delta T_{s,g}^{max} = \frac{\Delta T_{ad}}{1 - u_w/u_t} \tag{1}$$

The thermal wave u_t is determined by

$$u_t = \frac{\varepsilon \rho_g c_g u_g}{(1-\varepsilon)\rho_s c_s} \tag{2}$$

where $\rho_g c_g$ and $\rho_s c_s$ are the heat capacities of the gas and solid, respectively, u_g the gas velocity; ε the porosity of the packed bed. Eq. (1) is deduced by neglecting heat loss to the surroundings. At the same time, the dimensionless combustion wave speed u is defined by the following expression using the one-temperature approximation:

$$u = u_w/u_t = 1 - \left\{ \left(\frac{\Delta T_{ad}}{\Delta T_{s,i}} \right)^2 - \frac{4\beta a}{h_v} \right\}^{0.5} \tag{3}$$

where h_v is the convective heat exchange coefficient between the gas and solid phases; a is a dimensionless parameter. Subsequently, Kennedy et al. [12] show that this simple linear approximation could be improved by taking into account the temperature dependence of

$$c_p = c_p(T_0)\{1 + z(T - T_0)\}$$

to yield

$$u/u_t = (1 - \Delta T_{ad}/\Delta T_{max}) + (z/2T_{max}) * \{1 - (\Delta T_{ad}/\Delta T_{max})^2\}$$

In order to predict the combustion wave velocity and temperature distributions in the packed bed, Foutko et al. [6] suggested two parameters, i.e. the ignition temperature $T_{s,i}$ and the effective coefficient β for the heat exchange with the surroundings at experimental conditions. To validate the analytical solution, Foutko et al. [6] simulated the experiments of Zhandok et al. [1] applying a one-dimensional two-phase model with one-step kinetics. In their study, radiation was taken into account by an effective conductivity while gas phase transport was neglected.

Kennedy et al. [2] analyzed chemical structures of methane–air filtration combustion waves in a range of equivalence ratios from 0.2 to 2.5. Downstream, upstream, and standing waves were observed in the experiments. For equivalence ratios in the range of 0.45—1.7 at an inlet velocity of 0.25 m/s, downstream wave propagation occurred, this corresponds to the superadabatic combustion. With further increasing (>1.7) or decreasing (<0.45) the equivalence ratio, the regime of propagation changed to upstream and the maximum temperature in the packed bed was no longer higher than the adiabatic temperature for the specific inlet mixtures. The accompanying numerical simulation considered a fully developed steady combustion wave using an one-temperature model. The GRI1.2 methane oxidation mechanism was used in their model and the gas mixture thermal dispersion effect was included.

Hoffmann et al. [4] experimentally studied the behavior of a reciprocating superadabatic combustion system and the combustible limit was extended to an extremely low equivalence ratio of 0.026 for methane/air mixtures. The combustion wave was confined in the porous burner by periodically changing the directions of the flow. During the positive half cycle, the combustion wave traveled at a roughly constant speed from the upstream side of the porous media towards the downstream end.

Henneke and Ellzey [8] investigated low-velocity filtration combustion of lean methane/air mixtures in porous media using an one-dimensional model with detailed chemistry. Gas-phase dispersion effect was taken into account. Results showed that the gas-phase dispersion affected the wave speed significantly only at higher equivalence ratios.

Recently, Bubnovich et al. [7] presented analytical solutions for temperature and mass fractions of methane/air mixture combustion in a packed bed. The solutions were built in three different regions, i.e. the pre-heating region, the reaction region and the one of combustion products. Based on the solutions, the extension of the reaction region, the ignition temperature and combustion wave speed were also predicted. In their analysis an one-temperature model was employed and the methane oxidation mechanism was reduced to a global chemical reaction in a single step.

It is obvious that no matter the gas flow is constantly uni-directional or periodically changed in directions there exist two relevant parameters in the LVR of filtration combustion, namely, a nearly constant wave speed and a maximum temperature, as demonstrated by experiments [1–4] and analytical solutions [6,7]. The combustion wave speed u_w and the maximum temperature (T_{max}) represent major characteristics of filtration combustion and there should be a close relationship between them. Nevertheless, in spite of the extensive studies mentioned above, there are few researches focused on this relationship. In an early study (1966), Soete [13] experimentally measured combustion wave speed through a packed bed of sand for methane/oxygen/nitrogen mixtures. An equation system was established in a semi-empirical manner, which permits the prediction of the combustion wave speed and its final temperature as a function of the flow rate. However, an analytical solution to this relationship is still needed, which is objective of the present work.

In the following section, we formulate a mathematical model of filtration combustion in porous media and discuss effects of important control parameters on u_w and T_{max} in the wave. The performance of heat recirculation in the combustion zone is subsequently analyzed by examining the balance between different terms in the gas and solid energy equations. Under the assumption that the reaction zone is a flame sheet with an infinitesimal thickness, a relationship between u_w and T_{max} in the wave is obtained. It is theoretically confirmed that the superadiabatic effect is a result of the overlapping of the thermal wave and combustion wave. Then, by means of the laminar flame theory [14], the reaction zone is assumed to be a narrow region. Consequently, another relationship between u_w and T_{max} in the wave is deduced. Thus a closed analytical solution for u_w and T_{max} is presented. Finally, the results of our analysis and numerical simulation are validated against available experimental data from the literature.

2. Mathematical model

2.1. Problem formulation

An inert porous burner tested by Zhandok et al. [1] was considered in this study. Fig. 1 shows the geometry of the burner used in our simulations and later analysis. The burner consists of a quartz tube with an internal diameter of $D = 76$ mm and is packed with solid alumina pellets of 5.6 mm in diameter. Insulation layer surroundings the tube was made to reduce heat loss to the surroundings.

2.2. Governing equations

The fact that thick insulation layers surrounded the inside and outside of the burner wall makes the radial temperature gradient inside the burner negligible and an one-dimensional model is applicable for simulations. Nevertheless, the heat loss to the surroundings was considered in computations and assumed to be proportional to the temperature difference ($T_s - T_0$) by the factor β [15]. To simplify computations, the following assumptions were introduced:

(1) Porous media filled in the packed bed are noncatalytic, homogeneous and optically thick.
(2) The working gas is non-radiating. Gas flow in porous media is laminar and pressure loss in the burner is neglected.
(3) The diffusion effect of species in the gas mixture is not considered both in our simulations and later theoretical analysis.

Under these assumptions, the conservation equations for mass, species, as well as gas and solid temperatures can be expressed as follows:

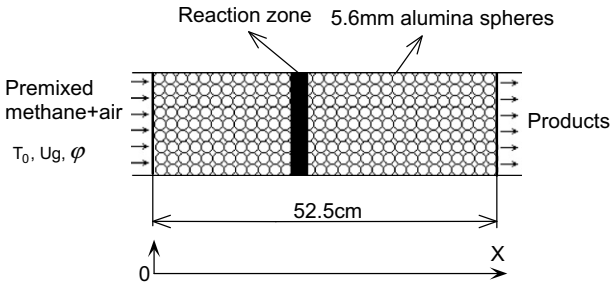

Fig. 1. Schematic diagram of the porous burner.

$$\frac{\partial(\varepsilon\rho_g)}{\partial t}+\frac{\partial(\rho_g u_g)}{\partial x}=0 \tag{4}$$

$$\varepsilon\rho_g\frac{\partial Y_i}{\partial t}+\varepsilon\rho_g u_g\frac{\partial Y_i}{\partial x}+\varepsilon\dot{\omega}_i=0 \tag{5}$$

$$\varepsilon\rho_g c_g\frac{\partial T_g}{\partial t}+\varepsilon\rho_g c_g u_g\frac{\partial T_g}{\partial x}=\varepsilon\frac{\partial}{\partial x}\left(\lambda_g\frac{\partial T_g}{\partial x}\right)+h_v(T_s-T_g)+\varepsilon Q\dot{\omega}_{CH_4} \tag{6}$$

$$(1-\varepsilon)\rho_s c_s\frac{\partial T_s}{\partial t}=(\lambda_s+\lambda_{rad})\frac{\partial^2 T_s}{\partial x^2}+h_v(T_g-T_s)-\beta(T_s-T_0) \tag{7}$$

where Q is the low heating value of fuel (in this study: methane).

The volumetric heat transfer [8] between the solid and gas phases, for the packed bed of alumina pellets is given by

$$h_v=Nu_v\times\lambda_g/d^2,\quad Nu_v=2+1.1Pr^{1/3}Re^{0.6} \tag{8}$$

where d is average diameter of the pellets. Gas densities were computed from the ideal gas equation of state for a multicomponent mixture

$$P=\rho_g RT_g/\overline{W} \tag{9}$$

Radiation is an importance heat transfer mechanism in the solid phase of packed bed, it enhances the heat transfer in the bed and broadens the reaction zone. The extended reaction zone exhibit intense surface radiation from the packing material but due to multiple reflections is essentially contained within an approximate length equal to the tube diameter. Thus the gas in this region can be treated as a thick gas for computation. For simplicity a radiation term is added to the solid thermal conductivity (λ_s) by a radiant conductivity model [16]:

$$\lambda_{rad}=(32\varepsilon\sigma d/9(1-\varepsilon))T_s^3 \tag{10}$$

where σ is Stephan–Boltzmann constant. For convenience in later theoretical analysis, we combine the solid conduction and radiation conductivity as $\lambda_{eff}=\lambda_s+\lambda_{rad}$.

The reaction of methane combustion is described by a single-step first-order Arrhenius type expression [15]:

$$\dot{\omega}_{CH_4}=\rho_g Y_{CH_4}A\exp(-E/RT_g) \tag{11}$$

2.3. Boundary conditions

The following boundary conditions are considered in the computations:

At the inlet:

$$T_g=300\text{ K},\quad Y_{CH_4}=Y_{CH_4,in},\quad Y_{O_2}=Y_{O_2,in}$$

At the outlet:

$$\frac{\partial T_g}{\partial x}=\frac{\partial T_s}{\partial x}=\frac{\partial Y_{CH_4}}{\partial x}=\frac{\partial Y_{O_2}}{\partial x}=0$$

2.4. Initial conditions and solution

The solid temperature was initialized according to the experimentally measured temperature profile [1]. To allow the gas and solid phases have own temperatures, user-defined functions (UDF) and scalars (UDS) were implemented and incorporated into the commercial CFD code FLUENT6.1. A mesh independence test of the computational results was conducted and an uniform 525×38 mesh was used for all computations. A residual error of 10E−6 for energy equations and 10E−3 for all other equations were taken as convergence criterions. The thermophysical properties of alumina pellets were taken to be constants [16], while gas properties varied with the gas species and temperature.

3. Computational results and discussion

3.1. Stable self-sustaining combustion wave

Typical gas and solid temperature profiles along the packed bed axis obtained from numerical solution under the experimental conditions of Zhdanok et al. [1] with a gas velocity of $u_g=0.43$ m/s and an equivalence ratio of $\varphi=0.153$ are shown in Fig. 2, in which the experimental results are also presented for comparison. We can see clearly a series of stable and self-sustaining combustion waves with a time interval of 300 s. As time goes on, the high temperature zones for both the gas and solid phases are broadened as the wave propagates because chemical energy is continuously input into the combustion zone. However, both u_w and T_{max} remain almost unchanged throughout the process. The numerical result shows a qualitative agreement with the experiment. There is a discrepancy in the maximum temperature, which might be attributed to the uncertainties in the thermal properties of the packed bed as well as to the global methane oxidation mechanism used in the simulation. Furthermore, the superadiabatic temperature in the combustion wave is clearly demonstrated in Fig. 2. The equivalence ratio under consideration in this case ($\varphi=0.153$) could not support a

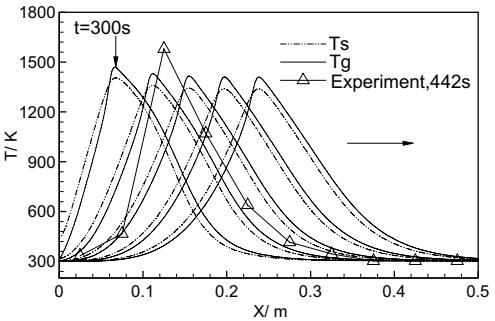

Fig. 2. Propagation of a stable combustion wave in porous media ($\varphi=0.153, u_g=0.43$ m/s, $\beta=1000$ W/m^3 K, $\Delta t=300$ s).

flame in an open tube, according to the experimental results by Mare et al. [17]. However, in our case there is a stably propagating combustion wave in the packed bed and the predicted T_{max} is approximately 2.8 times the adiabatic temperature of the inlet mixture, indicating a prominent superadiabatic effect.

3.2. Heat recirculation in flame zone

As mentioned above, a mixture with an equivalence ratio of 0.153 cannot support a flame in an open tube, whereas a combustion wave is able to propagate throughout the entire porous medium burner at the same inlet condition. This is due to the self-organizing energy feedback provided by the porous medium. To deepen the understanding of the heat recirculation effect in flame zone induced by the porous media, we examine the relative magnitudes of the different terms in the gas and solid energy equations, as shown in Fig. 3a and b. Here, the energy budget is normalized by the maximum heat release in the packed bed for the case of $\varphi = 0.2$ and $u_g = 0.43$ m/s. Fig. 3a shows that the energy release by chemical reaction is mostly balanced by advection and the rest is by conduction and convection (the heat exchange between the gas and the solid: the fourth term in the normalized Eq. (6)). In the pre-heat and thermal relaxation zones of the flame, heat transfer from solid to gas is balanced by advection. In the pre-heat zone, the gas is effectively preheated by convection while gas loses heat to the solid in the thermal relaxation zone. Fig. 3b demonstrates that the enthalpy feedback is provided mainly via convection and radiation.

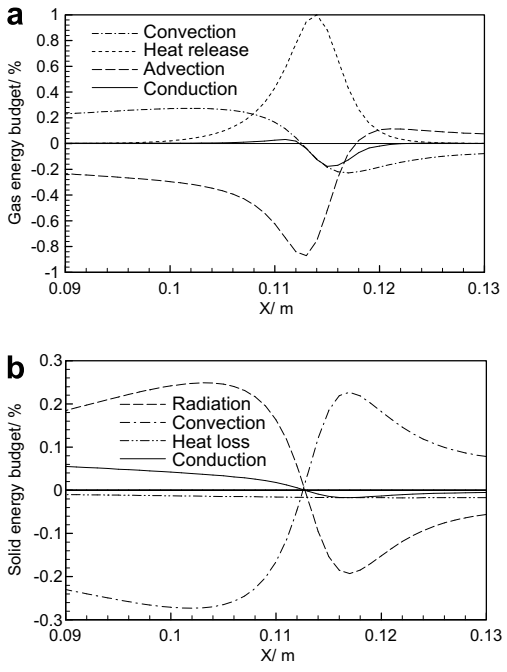

Fig. 3. Energy budget in porous media burner flame ($\varphi = 0.2$, $u_g = 0.43$ m/s, $\beta = 600$ W/m^3 K). (a) Gas phase in flame zone; (b) solid phase in flame zone.

Through these transport processes the heat release from the reaction is redistributed and a heat feedback from high temperature gas product to the unburnt mixture is realized. From Fig. 3b, it can be found that the heat loss to the surroundings is relative small and negligible in the whole flame zone.

3.3. Influence of porous media properties and inlet mixture

The sensitivity of the combustion wave to the heat capacity of the porous medium is shown in Fig. 4, in which the combustion wave velocity u_w and the maximum temperature T_{max} across the wave are plotted against equivalence ratio. With increasing equivalence ratio, u_w decreases because more fuel has to be consumed, while T_{max} increases due to larger heat input to the system. It is remarkable that the heat capacity of the porous media has a significant effect on u_w. When the heat capacity is settled to 0.5 times, then u_w is as large as almost 2 times of the original value. At the same time it is shown that T_{max} is almost independent of the heat capacity of the packed bed. These results are consistent with theoretical predictions [1]. As shown in Eq. (2), the thermal wave speed u_t is inversely proportional to the heat capacity of the solid packed bed. On the other hand, numerical predictions indicate that u_w is directly proportional to the heat capacity of the packed bed. Thus, from Eq. (1) it can be concluded that T_{max} keeps approximately constant when the heat capacity is changed under the condition that the heat loss to the surroundings is ignored.

According to Ref. [11], a strong interphase heat exchange in the zone of chemical transformation and a combustion wave velocity of about 0.1 mm/s are typical for the LVR. To examine the importance of the convective heat transfer (h_v) to u_w, extensive simulations were performed at the same condition as that shown in Fig. 4 ($\varphi = 0.153$–0.5, $u_g = 0.43$ m/s and $\beta = 600$ W/m^3 K). Results indicate that increasing convective heat transfer (predicted by Eq. (6)) by 10 times induces a slight decrease in u_w (~20%) when the equivalence ratio is less than 0.2. With further increasing equivalence ratio from 0.2 to 0.5, a decrease about 40% in u_w is found. Hence, it can be con-

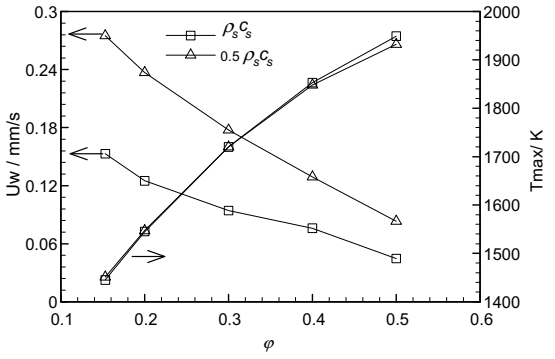

Fig. 4. The influence of heat capacity on u_w and T_{max}, ($u_g = 0.43$ m/s, $\beta = 600$ W/m^3 K).

cluded that the convection heat transfer has a weak influence on u_w.

The thermal conductivity of the packed bed has, theoretically, important influence on the behavior of combustion wave [8] and the conductivity is in turn greatly dependent on the specifics of the packing. Unfortunately, the detailed specifics of the bed in the experiment of Zhdanok et al. [1] are not available, such as the packing force applied. Thus we had to use values from the literature for the heat conductivity, which brought some uncertainties in the computation. Fig. 5 shows the predictive influence of the solid heat conduction on u_w and T_{max}. With increasing solid conductivity, the conductive heat fluxes from the hot flame zone to the colder parts of the burner increases, i.e. the heat feedback from the flame front is enhanced. As a consequence, the temperature peak T_{max} in the flame zone becomes lower. The T_{max} for the case with a solid conductivity $\lambda_s = 0.2$ is higher by 76 K than that for $\lambda_s = 1.3$ at the equivalence ratio of 0.153. This indicates that it is advantageous to use a porous medium with lower heat conductivity in the burner for realization of an extremely lean combustion, as in this way a higher combustion temperature can be attained. Another consequence induced by larger solid conductivity is an increase in the combustion wave speed u_w. However, it is shown by computations that solid conductivity has little influence on u_w and T_{max} when the equivalence ratio is larger than 0.3.

It should be noted here that in reality an effective conductivity depends to a great extent upon the packing characteristics and the conductivity of the packing spheres can be varied over a couple of orders of magnitude. As a result, the computed effect of the thermal conductivity might be within the experiment uncertainty and therefore not significant.

Fig. 6 describes the influence of heat loss on u_w and T_{max}. As expected, increasing heat loss to the surroundings leads to an increase in the wave speed and a decrease in the maximum temperature over the investigated range of equivalence ratio. Calculation results show that in the equivalence ratio range of 0.153–0.2, the heat loss has significant effect on wave propagation. For a given larger heat

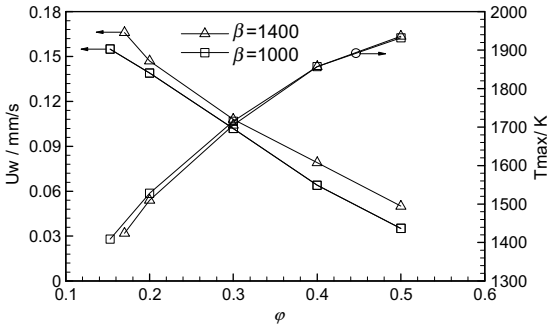

Fig. 6. The influence of heat loss on u_w and T_{max} ($u_g = 0.43$ m/s).

loss factor ($\beta = 1400$ W/m^3 K), a lean mixture ($\varphi = 0.153$) will be ignited and the wave can initially propagate downstream for a short time period, but heat losses will cause a gradual decay of T_{max} and eventually lead to an extinction. Consequently, the combustion wave cannot propagate throughout the burner. This corresponds to the extinction limit of wave propagation induced by heat loss. However, by increasing equivalence ratio to 0.17, a steadily traveling combustion wave is obtained and it propagates continuously to the burner exit. On the other hand, the mixture of lower equivalence ratio ($\varphi = 0.153$) can also stably propagate at a relative lower heat loss ($\beta = 1000$ W/m^3 K). However, with further increasing in equivalence ratio from 0.3 to 0.5, the heat loss has little influence on T_{max}.

Fig. 7 depicts gas and solid temperature profiles for three different equivalent ratios at the time of 1500 s. It is obvious that the leaner the mixture is, the faster the wave propagates. The temperature differences between the gas and solid phases are relative small except for the reaction zone. This indicates that the thermal non-equilibrium between the two phases is relative low off the flame zone due to strong interstitial heat transfer. At the same time, the efficient heat transfer ensures the coupling between the thermal wave and combustion wave. The interphase temperature differences within the flame zone are getting larger with increasing equivalence ratio. Correspondingly, using an one-temperature model in the reaction zone may result in large discrepancies when the mixture is not extremely lean.

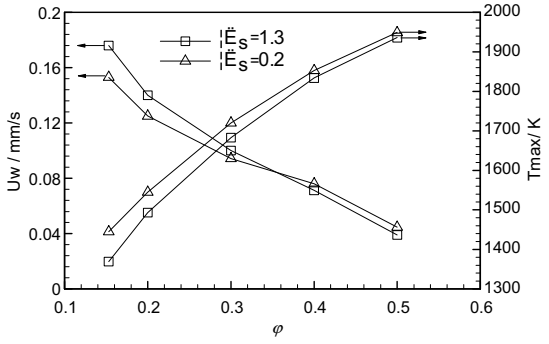

Fig. 5. The influence of heat conductivity on u_w and T_{max}, ($u_g = 0.43$ m/s, $\beta = 600$ W/m^3 K).

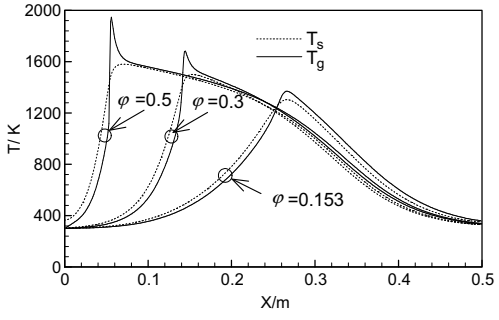

Fig. 7. The influence of equivalence ratio on u_w and T_{max} ($u_g = 0.43$ m/s, $\beta = 1000$ W/m^3 K).

4. Theoretical analysis

4.1. Overlapping of thermal wave and combustion wave

To clarify the mechanism of the overlapping of the thermal wave and combustion wave, a theoretical analysis of the temperature distribution in the burner is performed. To simplify the problem, we assume that heat exchange between the gas and solid phases takes place very fast, so that their temperatures rapidly equilibrate. Thus, we need only consider a single temperature field. The thermal conductivity and capacity of the porous media are considered to be large relative to those of gas mixtures. The heat loss to the surroundings is ignored. In the following analysis the reaction sheet approximation is employed, consequently, the reaction rate may be replaced by a Dirac δ-function. Under the one-temperature approximation, Eqs. (6) and (7) can be combined and then divided by $(1-\varepsilon)\rho_s c_s$, we obtain the temperature distribution in the burner:

$$\frac{\partial T}{\partial t}+u_t\frac{\partial T}{\partial x}=\Omega\frac{\partial^2 T}{\partial x^2}+\frac{\varepsilon\rho_g c_g\Delta T_{ad}\delta(x)}{(1-\varepsilon)\rho_s c_s} \tag{12a}$$

$$T(x,0)=T^0(x) \tag{12b}$$

where $\Omega=\frac{\lambda_{eff}}{(1-\varepsilon)\rho_s c_s}$.

The initial temperature distribution $T(x,0)$ is assumed to be the same as the initial pre-heating temperature profile in the experiment of Zhandok et al. [1].

Eq. (12) can be solved by a Fourier transformation. To do this, the temperature T has to be replaced by $T-T_0$ to ensure the following boundary condition:

$$x\to-\infty,+\infty,\quad T=0;\quad \frac{dT}{dx}=0 \tag{13}$$

Eq. (12) is an initial value problem and its analytical solution can be found which is divided into two parts (for detail of the solution process see Appendix A):

$$T(x,t)=T_1(x,t)+T_2(x,t) \tag{14}$$

where

$$T_1(x,t)=\frac{1}{\sqrt{4\pi\Omega t}}\int_{-\infty}^{+\infty}(T^0(\xi)-T_0)\exp\left(-\frac{(x-\xi-tu_t)^2}{4\Omega t}\right)d\xi+T_0,$$

$$T_2(x,t)=\frac{\varepsilon\rho_g c_g\Delta T_{ad}}{(1-\varepsilon)\rho_s c_s}\int_0^t\frac{1}{\sqrt{4\pi\Omega\tau'}}\exp\left(-\frac{(x-u_t\tau')^2}{4\Omega\tau'}\right)d\tau'$$

Eq. (12) and its solution are similar to those given by Ref. [18], in which Aldushin et al. presented temperature fields for the filtration combustion between a reactive filtering gas and solid fuel. Eq. (14) shows that the temperature in the burner is induced jointly by both the thermal wave and the combustion wave. The first term in the right hand of Eq. (14) accounts for the effect of the initial temperature field $T(x,0)$ on the temperature distribution, and the second term represents the effect of reaction heat. The effect of the initial temperature on the temperature distribution decays as time goes on. Eq. (14) demonstrates theoretically that the superadiabatic effect is a result of the overlapping of the thermal and combustion waves in the porous media under certain conditions.

4.2. Analysis of combustion wave

In the following a theoretical analysis of a combustion wave in porous medium is presented. Considering a premixed fuel/air mixture that enters the packed bed with an equivalence ratio φ and initial temperature T_0 as well as a mixture inlet velocity u_g. In our one-dimensional model a fully developed wave moving at a constant speed u_w in the porous bed is examined. Under the reaction sheet assumption the reaction front can be seen as infinite thin and, as noted above, the reaction rate may be represented by a Dirac δ-function. Thus, in a reference frame of a new coordinate $\xi=x-u_w t$ which is attached to the reaction front moving in the x-direction with velocity u_w, Eqs. (5) and (12a) are transformed as (noting that $u_w\ll u_g$)

$$\rho_g u_g\frac{dY_{fuel}}{d\xi}+\dot\omega_{fuel}=0 \tag{15}$$

$$(\varepsilon\rho_g c_g u_g-(1-\varepsilon)u_w\rho_s c_s)\frac{dT}{d\xi}=\lambda_{eff}\frac{d^2T}{d\xi^2}+\varepsilon\rho Q\dot\omega_{fuel}-\beta(T-T_0) \tag{16}$$

Here the heat loss is included in Eq. (16). The following dimensionless parameters and variables are introduced [1]:

$$\chi=\frac{\xi}{\varepsilon\rho_g c_g u_g},\quad \Theta=\frac{T-T_0}{\Delta T_{max}},\quad a=\frac{\lambda_{eff}}{(\varepsilon\rho_g c_g u_g)^2},$$

$$\Delta T_{max}=T_{max}-T_0,\quad u=\frac{u_w}{u_t}$$

After a variable substitution, Eq. (16) is rewritten as

$$a\frac{d^2\Theta}{d\chi^2}-(1-u)\frac{d\Theta}{d\chi}-\beta\Theta+\frac{\Delta T_{ad}\delta(\chi)}{\Delta T_{max}}=0 \tag{17}$$

Boundary conditions for Eq. (17) are

$$\chi\to-\infty,+\infty,\quad \Theta=0;\quad \frac{d\Theta}{d\chi}=0 \tag{18}$$

$$\Theta(-0)=\Theta(+0)=1 \tag{19a}$$

$$\Theta'(0^+)-\Theta'(0^-)=\frac{\Delta T_{ad}}{a\Delta T_{max}} \tag{19b}$$

Eq. (17) is a two-order linear ordinary differential equation with constant coefficients. The corresponding characteristic polynomial for its homogeneous counterpart is

$$ak^2-(1-u)k-\beta=0 \tag{20}$$

Eq. (20) has two characteristic roots:

$$k_{1,2}=\frac{1}{2a}(1-u)\pm\frac{1}{2a}\left[(1-u)^2+4a\beta\right]^{0.5} \tag{21}$$

where $k_1>0$ and $k_2<0$.

Correspondingly, Eq. (17) with the boundary conditions (18) and (19) has a solution in the following dimensionless form:

$$\chi < 0,\ \ \Theta(\chi) = e^{k_1\chi};\quad \chi > 0,\ \ \Theta(\chi) = e^{k_2\chi} \tag{22}$$

The maximum temperature T_{max} in the wave is determined from (19) and (22)

$$T_{max} = \frac{\Delta T_{ad}}{\left[(1-u)^2 + 4a\beta\right]^{0.5}} + T_0 \tag{23}$$

Eq. (23) presents a relationship between two variables, u_w and T_{max}.

In the above analytical solution, the reaction zone thickness is disregarded in order to be able to integrate the energy equation following previous researchers [1,6]. In reality, the reaction zone in the PM is quite thick. However, as we can observe from measured temperature distributions in the combustion wave (Fig. 2), the temperature has always a localized peak value, i.e. a maximum and it is getting down rapidly in the both sides of the peak. This means that the reaction takes place most intensively in a limited narrow area around the front. Based on this observation, the flame sheet approximation can be considered justified. Recently, Bubnovich et al. [7] presented an analytical solution for the filtration combustion in a packed bed in which the longitudinal extension of the reaction region was considered. In the later theoretical analysis of this work we will also treat the flame thickness as a narrow reaction zone.

To find both of u_w and T_{max}, we have to establish another expression. To do this we employ an approach from the laminar premixed flame theory [14], according to which, the entire flame zone can be divided into two regions: the pre-heating region, $\xi_p < \xi < \xi_i$, and the reaction region, $\xi_i < \xi < \xi_{max}$. The subscripts p, i and max, denote the initial, ignition and maximum positions in the ξ-direction, respectively.

Because of the large energy of activation of hydrocarbon fuels, most of the combustion reactions take place at temperatures near the maximum flame temperature and indeed the ignition temperature T_i is very close to the flame temperature [14]. We assume that fuel is completely consumed in the reaction zone. This means that fuel cannot leak through the combustion wave. On the other hand, chemical reactions are neglected in the pre-heating zone. Consequently, Eq. (16) can then be reduced to

$$B\frac{dT}{d\xi} = \lambda^{p}_{eff}\frac{d^2T}{d\xi^2} - \beta(T - T_0) \tag{24}$$

where $B = (\varepsilon\rho_g c_g u_g - (1-\varepsilon)u_w\rho_s c_s)$, the superscript p and the later used r denote the averaged value in the corresponding pre-heating and reaction regions, respectively. In the pre-heating region, the boundary conditions for Eq. (24) are

$$\xi = \xi_p,\ \ \frac{dT}{d\xi} = 0,\ \ T = T_0,\ \ Y_{fuel} = Y^0_{fuel};\quad \xi = \xi_{i-},\ \ Y_{fuel} = Y^0_{fuel} \tag{25}$$

Integrating Eq. (24) from $\xi = \xi_p$ to $\xi = \xi_{i-}$ over the pre-heating region with the boundary conditions (Eq. (25)) yields

$$\left.\frac{dT}{d\xi}\right|_{\xi=i-} = \frac{B(T_i - T_0)}{\lambda^{p}_{eff}} + \frac{\beta}{\lambda^{p}_{eff}}\int_{\xi_p}^{\xi_{i-}}(T - T_0)d\xi \tag{26}$$

In Eq. (26), the variable $T - T_0$ varies from zero to $T_i - T_0$ over the integrated interval and we take its average value as $(T_i - T_0)/2$. Thus, Eq. (26) can be reduced to

$$\left.\frac{dT}{d\xi}\right|_{\xi=i-} = \frac{(2B + \beta\Delta_p)}{2\lambda^{p}_{eff}}(T_i - T_0) \tag{27}$$

where $\Delta_p = \xi_{i-} - \xi_p$. Under the assumption that the slope of the temperature curve is linear in the pre-heat region, Δ_p could be approximated by the expression:

$$\Delta_p = (T_i - T_0)\Big/\left.\frac{dT}{d\xi}\right|_{\xi=i-} \tag{28}$$

Substituting Eq. (28) into Eq. (27) and eliminating unreal value, we obtain:

$$\left.\frac{dT}{d\xi}\right|_{\xi=i-} = \frac{(T_i - T_0)}{2\lambda^{p}_{eff}}\left(B + (B^2 + 2\beta\lambda^{p}_{eff})^{0.5}\right) \tag{29}$$

In the reaction region, the convective term can be ignored according to the laminar flame theory. Furthermore, if heat loss is not taking into account ($\beta = 0$), Eq. (16) is then reduced to the following expression:

$$\lambda^{r}_{eff}\frac{d^2T}{d\xi^2} + \varepsilon Q\dot{\omega} = 0 \tag{30}$$

The corresponding boundary conditions for Eq. (30) are

$$\xi = \xi_{i+},\ \ \left.\frac{dT}{d\xi}\right|_{\xi=i-} = \left.\frac{dT}{d\xi}\right|_{\xi=i+};\quad Y_{fuel} = Y^0_{fuel} \tag{31a}$$

$$\xi = \xi_{max},\ \ \left.\frac{dT}{d\xi}\right|_{\xi_{max}} = 0;\quad Y_{fuel} = 0 \tag{31b}$$

Substituting Eq. (30) into Eq. (15) and integrating it from an arbitrary point in the reaction region to ξ_{max} with boundary condition (Eq. (31)), we obtain

$$Y_{CH_4} = \frac{\lambda^{r}_{eff}}{\varepsilon\rho_g u_g Q}\frac{dT}{d\xi} \tag{32}$$

Substituting Eq. (32) into Eq. (30) yields

$$\frac{d^2T}{d\xi^2} + \frac{A}{u^{r}_{g}}\frac{dT}{d\xi}\exp(-E/RT) = 0 \tag{33}$$

Integrating Eq. (33) from ξ_i to ξ_{max} in the reaction region with boundary condition (Eq. (31)) yields

$$\left.\frac{dT}{d\xi}\right|_{i+} = \frac{A}{u^{r}_{g}}\int_{T_i}^{T_{max}}\exp(-E/RT)dT \tag{34}$$

We integrate Eq. (34) as Ref. [14] and introduce following dimensionless parameters and variables [14]:

$$\theta = \frac{T - T_{\max}}{T_{\max} - T_i}, \quad \gamma = \frac{RT_{\max}^2}{E(T_{\max} - T_i)}, \quad \alpha = \frac{RT_{\max}}{E} \tag{35}$$

Substituting Eq. (35) into Eq. (34) and integrating it, one obtains

$$\left.\frac{dT}{d\xi}\right|_{i+} = \frac{ART_{\max}^2}{u_g^r E} \exp(-E/RT_{\max})(1 - \exp(-1/\gamma)) \tag{36}$$

Now, substituting Eqs. (29) and (36) into Eq. (31), we obtain finally another relationship between u_w and $T_{\max}$:

$$u_w = u_t + \frac{(B^2 + 2\beta\lambda_{\text{eff}}^p)^{0.5}}{(1-\varepsilon)\rho_s c_s} - \frac{2\lambda_{\text{eff}}^p ART_{\max}^2}{u_g^r E(T_i - T_0)(1-\varepsilon)\rho_s c_s} * \exp(-E/RT_{\max}) \times \left(1 - \exp\left(\frac{E(T_i - T_{\max})}{RT_{\max}^2}\right)\right) \tag{37}$$

Eq. (37) may be reduced to a simpler form when the heat loss is ignored:

$$u = 1 - \frac{\varepsilon\rho_g c_g \lambda_{\text{eff}}^p ART_{\max}^2}{u_g^r E(T_i - T_0)} * \exp(-E/RT_{\max}) \left(1 - \exp\left(\frac{E(T_i - T_{\max})}{RT_{\max}^2}\right)\right) \tag{38}$$

Eqs. (23) and (37) build a closed solution for the combustion wave speed u_w and the maximum temperature $T_{\max}$ and can be solved easily with a short computer code.

4.3. Analysis of the theoretical results of combustion waves

In solving Eqs. (23) and (37), variations of gas thermophysical properties with temperature are taken into account in such a simple manner that their average values over a corresponding specific zone are used. The gas mixture properties are approximated by those of air due to relative smaller content of fuel in the mixture. The gas properties are taken as their values at the adiabatic temperature of the inlet fuel/air mixture except for the reaction zone. In the flame zone, the gas properties are specified as the average values between their values at the ignition temperature and those at the maximum temperature. In addition, the properties of the porous media are assumed to be constants with respect to the temperature as in the above numerical simulations. For simplification, the ignition temperature for methane is given as [14]

$$T_i = 0.75T_{\max}$$

For a theoretically predicted combustion wave speed u_w, the temperature field in the packed bed defined by Eq. (22) now can be solved. Fig. 8 presents a comparison between the temperature profiles given by theory and by experiment. The entire temperature profile is divided into two parts by $\chi = 0$ (corresponds to $x = 0.1$ approximately in Fig. 8), i.e. the pre-heat region and the reaction region.

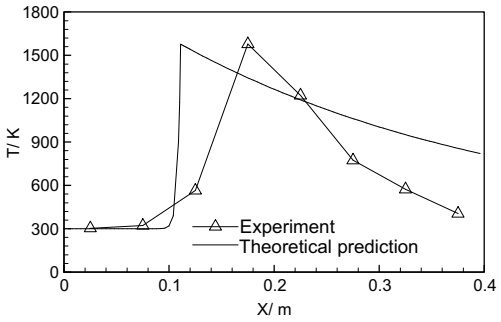

Fig. 8. Comparison between the temperature profiles given by theory prediction and experimental results ($\varphi = 0.15$, $u_g = 0.43$ m/s, $\beta = 600$ W/m^3 K).

The temperature distribution is continuous but not smooth in comparison with the numerical results (see e.g. Figs. 2 and 7). In addition, the convective heat exchange between the gas and solid phases cannot be predicted due to the assumption of the local thermal equilibrium.

Fig. 9 shows the effect of the equivalence ratio on u_w for three different gas inlet velocities. Increasing the inlet mixture velocity leads to an increase in the wave speed. Varying the equivalence ratio seems to have significant influence on the combustion wave speed. The larger the equivalence ratio of the methane/air mixture is, the grater the combustion wave speed becomes.

Furthermore, the prediction results show that there exist two different combustion waves propagating in positive or negative directions, which correspond to wave speeds greater or less than zero, respectively. As shown in Fig. 9, a critical case of $u_w = 0$ is observed at the equivalence ratio of 0.582 for the inlet mixture velocity $u_g = 0.43$ m/s, indicating that the combustion wave stays and fixed at a certain position of the packed bed. When the equivalence ratio is greater than 0.582, the wave speed becomes negative, implying that the combustion wave propagates upstream in the opposite direction of the gas flow. In this case the superadiabatic effect is no longer realizable, instead, a subadiabatic combustion takes place, in which the maximum temperature in reaction zone is lower than the adiabatic flame temperature. Eq. (1) also indicates that when the thermal wave and combustion wave propagates in the same direction and the ratio u_w/u_t become

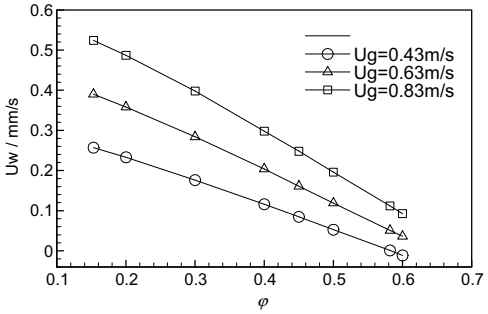

Fig. 9. Effect of the equivalence ratio on the wave speed for the three different gas inlet velocities ($\beta = 1000$ W/m^3 K).

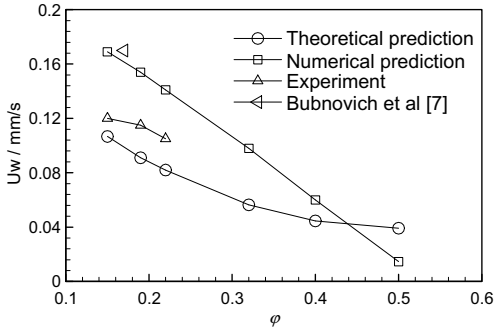

Fig. 10. Numerical simulation, theory prediction and experimental results of the u_w ($u_g = 0.29$ m/s, $\beta = 600$ W/m^3 K).

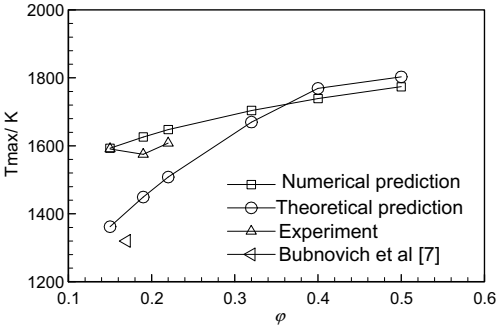

Fig. 11. Numerical simulation, theory prediction and experimental results of the T_{max} ($u_g = 0.29$ m/s, $\beta = 600$ W/m^3 K).

unity, the combustion temperature T_{max} is infinite, implying a maximal energy accumulation. Accordingly, it can be concluded that the prerequisite for superadiabatic combustion is that the combustion wave propagates in the same direction with the thermal wave. Figs. 10 and 11 show comparisons of our numerical and theoretical results to the experimental data [1,19] and theoretical solution by Bubnobich et al. [7]. Qualitative agreement between the numerical and theoretical model can be noted. The numerical and theoretical predicted u_w and T_{max} are, respectively, greater and less than the corresponding experimental results, as shown in Figs. 10 and 11. For comparison, similar analytical solutions from Ref. [7] are also indicated in Figs. 10 and 11.

5. Conclusion

Numerical simulation and theoretical analysis of low-velocity filtration combustion have been presented. Numerical results show that under lean mixture condition, the most important control parameter affecting the combustion wave speed u_w is the thermal capacity of the porous media in the packed bed combustor. On the other hand, the thermal capacities have weak influence on the maximum temperature T_{max}. A weak dependence of u_w and T_{max} on convective heat transfer is also demonstrated by the numerical calculation. Heat loss to the surroundings through the burner walls has influence on both the wave speed and the maximum temperature. To attain a higher combustion temperature, it is advantageous to arrange porous material with smaller conductivity in the reaction zone of the burner. In this way, a stable superadiabatic combustion is feasible even for extremely lean mixtures.

Based on the gas–solid thermal equilibrium assumption by using an one-temperature model, the solution of the temperature distribution in the burner has been found by a Fourier transformation and expressed as a sum of two parts: a thermal wave temperature field and a combustion wave one. This result reveals that the mechanism of superadiabatic combustion is attributed to the overlapping of the thermal wave and combustion wave under certain conditions.

Finally, based on the flame sheet assumption and laminar flame theory, two relationships between the wave speed and the maximum temperature across the wave are established and this leads to a closed solution. Qualitative agreements of the numerical simulation and theoretical analysis with the experimental results have been obtained.

Acknowledgements

The authors acknowledge the support to this work by the National Natural Science Foundation of China (NSFC Grant Nos. 50076005, 50476073).

Appendix A

The solution process of Eq. (12) is presented in the following. We rewrite Eq. (12a) and its initial condition here for convenience:

$$\frac{\partial T}{\partial t} + u_t \frac{\partial T}{\partial x} = \Omega \frac{\partial^2 T}{\partial x^2} + \frac{\varepsilon \rho_g c_g \Delta T_{ad} \delta(x)}{(1-\varepsilon)\rho_s c_s} \tag{12a}$$

$$T(x,0) = T^0(x) \tag{12b}$$

A new variable $W(x,t)$ is introduced as

$$T(x,t) = W(x,t) \exp\left(\frac{u_t}{2\Omega}x - \frac{u_t^2}{4\Omega}t\right) \tag{A.1}$$

Eq. (12a) then becomes

$$\frac{\partial W}{\partial t} = \Omega \frac{\partial^2 W}{\partial x^2} + g(x,t) \tag{A.2}$$

where

$$g(x,t) = \frac{\varepsilon \rho_g c_g \Delta T_{ad} \delta(x)}{(1-\varepsilon)\rho_s c_s} \exp\left(-\frac{u_t}{2\Omega}x + \frac{u_t^2}{4\Omega}t\right) \tag{A.3}$$

Correspondingly, Eq. (12b) becomes

$$W(x,0) = (T^0(x) - T_0) \exp\left(-\frac{u_t}{2\Omega}x\right) \tag{A.4}$$

We take Fourier transformation for $W(x,t)$ as

$$\overline{W}(\kappa,t) = \int_{-\infty}^{+\infty} W(x,t) e^{i\kappa x} dx$$

Substituting this expression into Eq. (A.2), one obtains

$$\frac{\mathrm{d}\overline{W}}{\mathrm{d}t} = -\Omega\kappa^2\overline{W} + \bar{g}(\kappa,t) \tag{A.5}$$

By Fourier transformation, Eq. (A.4) becomes

$$\begin{aligned}\overline{W}(\kappa,0) &= \bar{\varphi}(\kappa)\\ &= \int_{-\infty}^{+\infty}(T^0(x)-T_0)\exp\left(-\frac{u_\mathrm{t}}{2\Omega}x\right)\exp(\mathrm{i}\kappa x)\mathrm{d}x\end{aligned} \tag{A.6}$$

Eq. (A.5) has a solution in the following form:

$$\overline{W} = \bar{\varphi}(\kappa)\mathrm{e}^{-\Omega\kappa^2 t} + \int_0^t \bar{g}(\kappa,t)\mathrm{e}^{-\Omega\kappa^2(t-\tau)}\,\mathrm{d}\tau \tag{A.7}$$

We then take an inverse Fourier transformation of Eq. (A.7) as

$$W = F^{-1}\left[\bar{\varphi}(\kappa)\mathrm{e}^{-\Omega\kappa^2 t}\right] + F^{-1}\left[\int_0^t \bar{g}(\kappa,t)\mathrm{e}^{-\Omega\kappa^2(t-\tau)}\mathrm{d}\tau\right] \tag{A.8}$$

where

$$F^{-1}[\bar{\varphi}(\kappa)\mathrm{e}^{-\Omega\kappa^2 t}] = F^{-1}[\bar{\varphi}(\kappa)] * F^{-1}[\mathrm{e}^{-\Omega\kappa^2 t}]$$

$$F^{-1}[\bar{\varphi}(\kappa)] = (T^0(x)-T_0)\exp\left(-\frac{u_\mathrm{t}}{2\Omega}x\right)$$

$$F^{-1}[\mathrm{e}^{-\Omega\kappa^2 t}] = \frac{1}{\sqrt{4\pi\Omega t}}\exp\left(-\frac{x^2}{4\Omega t}\right)$$

The second term in Eq. (A.8) can be written as

$$\begin{aligned}F^{-1}[\bar{\varphi}(\kappa)\mathrm{e}^{-\Omega\kappa^2 t}] &= \frac{1}{\sqrt{4\pi\Omega t}}\int_{-\infty}^{+\infty}(T^0(x)-T_0)\\ &\quad\times\exp\left(-\frac{u_\mathrm{t}}{2\Omega}\xi\right)\exp\left(-\frac{(x-\xi)^2}{4\Omega t}\right)\mathrm{d}\xi\end{aligned}$$

The third term in Eq. (A.8)

$$\begin{aligned}F^{-1}\left[\int_0^t \bar{g}(\kappa,t)\mathrm{e}^{-\Omega\kappa^2(t-\tau)}\mathrm{d}\tau\right] &= \frac{1}{2\pi}\int_{-\infty}^{+\infty}\int_0^t \bar{g}(\kappa,t)\mathrm{e}^{-\Omega\kappa^2(t-\tau)}\mathrm{e}^{-\mathrm{i}\kappa x}\mathrm{d}\tau\mathrm{d}\kappa\\ &= \int_0^t \frac{1}{2\pi}\int_{-\infty}^{+\infty}\bar{g}(\kappa,t)\mathrm{e}^{-\Omega\kappa^2(t-\tau)}\mathrm{e}^{-\mathrm{i}\kappa x}\mathrm{d}\kappa\mathrm{d}\tau\\ &= \int_0^t F^{-1}\left[\bar{g}(\kappa,t)\mathrm{e}^{-\Omega\kappa^2(t-\tau)}\right]\mathrm{d}\tau\\ &= \int_0^t g(x,t) * F^{-1}\left[\mathrm{e}^{-\Omega\kappa^2(t-\tau)}\right]\mathrm{d}\tau\\ &= \int_{-\infty}^{+\infty}\int_0^t \frac{\varepsilon\rho_\mathrm{g}c_\mathrm{g}\Delta T_\mathrm{ad}\delta(\xi)}{(1-\varepsilon)\rho_\mathrm{s}c_\mathrm{s}}\\ &\quad\times\exp\left(-\frac{u_\mathrm{t}}{2\Omega}\xi+\frac{u_\mathrm{t}^2}{4\Omega}\tau\right)\frac{1}{\sqrt{4\Omega\pi(t-\tau)}}\\ &\quad\times\exp\left(-\frac{(x-\xi)^2}{4\Omega(t-\tau)}\right)\mathrm{d}\xi\mathrm{d}\tau\end{aligned}$$

by adding the second term to the third one in Eq. (A.8), one obtains

$$\begin{aligned}W &= \frac{1}{\sqrt{4\pi\Omega t}}\int_{-\infty}^{+\infty}(T^0(x)-T_0)\exp\left(-\frac{u_\mathrm{t}}{2\Omega}\xi\right)\\ &\quad\times\exp\left(-\frac{(x-\xi)^2}{4\Omega t}\right)\mathrm{d}\xi\\ &\quad+\int_0^t\int_{-\infty}^{+\infty}\frac{\varepsilon\rho_\mathrm{g}c_\mathrm{g}\Delta T_\mathrm{ad}\delta(\xi)}{(1-\varepsilon)\rho_\mathrm{s}c_\mathrm{s}}\exp\left(-\frac{u_\mathrm{t}}{2\Omega}\xi+\frac{u_\mathrm{t}^2}{4\Omega}\tau\right)\\ &\quad\times\frac{1}{\sqrt{4\Omega\pi(t-\tau)}}\exp\left(-\frac{(x-\xi)^2}{4\Omega(t-\tau)}\right)\mathrm{d}\xi\,\mathrm{d}\tau\end{aligned} \tag{A.9}$$

Substituting Eq. (A.9) into Eq. (A.1), we get

$$\begin{aligned}T(x,t) &= \frac{1}{\sqrt{4\pi\Omega t}}\int_{-\infty}^{+\infty}(T^0(x)-T_0)\exp\left(-\frac{(x-\xi-u_\mathrm{t}t)^2}{4\Omega t}\right)\mathrm{d}\xi\\ &\quad+T_0+\frac{\varepsilon\rho_\mathrm{g}c_\mathrm{g}\Delta T_\mathrm{ad}}{(1-\varepsilon)\rho_\mathrm{s}c_\mathrm{s}}\exp\left(\frac{u_\mathrm{t}}{2\Omega}x-\frac{u_\mathrm{t}^2}{4\Omega}t\right)\\ &\quad\times\int_0^t\int_{-\infty}^{+\infty}\delta(\xi)\exp\left(-\frac{u_\mathrm{t}}{2\Omega}\xi+\frac{u_\mathrm{t}^2}{4\Omega}\tau\right)\\ &\quad\times\frac{1}{\sqrt{4\Omega\pi(t-\tau)}}\exp\left(-\frac{(x-\xi)^2}{4\Omega(t-\tau)}\right)\mathrm{d}\xi\,\mathrm{d}\tau\end{aligned} \tag{A.10}$$

The last term in Eq. (A.10) can be reduced to

$$\frac{\varepsilon\rho_\mathrm{g}c_\mathrm{g}\Delta T_\mathrm{ad}}{(1-\varepsilon)\rho_\mathrm{s}c_\mathrm{s}}\int_0^t\frac{1}{\sqrt{4\Omega\pi(t-\tau)}}\exp\left(-\frac{(x-u_\mathrm{t}(t-\tau))^2}{4\Omega(t-\tau)}\right)\mathrm{d}\tau$$

Defining a new integration variable as $t-\tau=\tau'$, the last term in Eq. (A.10) can further be reduced to

$$\frac{\varepsilon\rho_\mathrm{g}c_\mathrm{g}\Delta T_\mathrm{ad}}{(1-\varepsilon)\rho_\mathrm{s}c_\mathrm{s}}\int_0^t\frac{1}{\sqrt{4\pi\Omega\tau'}}\exp\left(-\frac{(x-u_\mathrm{t}\tau')^2}{4\Omega\tau'}\right)\mathrm{d}\tau'$$

Thus we get $T(x,t)$ as

$$T(x,t) = T_1(x,t) + T_2(x,t) \tag{A.11}$$

where

$$\begin{aligned}T_1(x,t) &= \frac{1}{\sqrt{4\pi\Omega t}}\int_{-\infty}^{+\infty}(T^0(x)-T_0)\\ &\quad\times\exp\left(-\frac{(x-\xi-u_\mathrm{t}t)^2}{4\Omega t}\right)\mathrm{d}\xi+T_0\end{aligned} \tag{A.12}$$

$$T_2(x,t) = \frac{\varepsilon\rho_\mathrm{g}c_\mathrm{g}\Delta T_\mathrm{ad}}{(1-\varepsilon)\rho_\mathrm{s}c_\mathrm{s}}\int_0^t\frac{1}{\sqrt{4\pi\Omega\tau'}}\exp\left(-\frac{(x-u_\mathrm{t}\tau')^2}{4\Omega\tau'}\right)\mathrm{d}\tau' \tag{A.13}$$

References

[1] S.A. Zhdanok, L.A. Kennedy, G. Koester, Superadiabatic combustion of methane air mixtures under filtration in packed bed, Combust. Flame 100 (1997) 221–231.

[2] L.A. Kennedy, J.P. Bingue, A. Saveliev, A.A. Fridman, S.I. Foutko, Chemical structures of methane–air filtration combustion waves for fuel-lean and fuel-rich conditions, Proc. Combust. Inst. 28 (2000) 1431–1438.

[3] J.P. Bingue, A.V. Saveliev, A.A. Fridman, L.A. Kennedy, Hydrogen sulfide filtration combustion: comparison of theory and experiment, Exp. Therm. Fluid Sci. 26 (2002) 409–415.
[4] J.G. Hoffmann, R. Echigo, H. Yoshida, S. Tada, Experimental study on combustion in porous media with a reciprocating flow system, Combust. Flame 111 (1997) 32–46.
[5] Y. Yoshizawa, K. Sasaki, R. Echigo, Analytical study of the structure of radiation controlled flame, Int. J. Heat Mass Transfer 31 (1998) 311–319.
[6] S.I. Foutko, S.I. Shabunya, S.A. Zhdanok, Superadiabatic combustion wave in a diluted methane–air mixture under filtration in a packed bed, in: Twenty-Sixth Symposium (Int.) on Combustion, The Combustion Institute, Naples, 1996, pp. 3377–3382.
[7] V.I. Bubnovich, S.A. Zhdanok, K.V. Dobrego, Analytical study of the combustion waves propagation under filtration of methane–air mixture in a packed bed, Int. J. Heat Mass Transfer 49 (2006) 2578–2586.
[8] M.R. Henneke, J.L. Ellzey, Modeling of filtration combustion in a packed bed, Combust. Flame 117 (1999) 832–840.
[9] J.R. Howell, M.J. Hall, Ellzey, Combustion of hydrocarbon fuels within porous inert media, Prog. Energy Combust. Sci 22 (1996) 121–145.
[10] M.M. Kamal, A.A. Mohamad, Combustion in porous media, Proc. ImechE Part A: J. Power Energy 220 (2006) 487–508.
[11] V.S. Babkin, Pure Appl. Chem. 65 (1993) 335–344.
[12] L.A. Kennedy, A.A. Fridman, A.V. Saveliev, Superadiabatic combustion in porous media: wave propagation, instabilities, new type of chemical reactor, Int. J. Fluid Mech. Res. 2 (22) (1995) 1–27.
[13] G.D. Soete, Stability and propagation of combustion waves in inert porous media, in: Eleventh Symposium (Int.) on Combustion, The Combustion Institute, 1966, pp. 959–966.
[14] Irvin Glassman, Combustion, third ed., Academic Press Inc., 1996, pp. 132–139.
[15] F. Contarin, A.V. Saveliev, A.A. Fridman, L.A. Kennedy, A reciprocal flow filtration combustor with embedded heat exchangers: numerical study, Int. J. Heat Mass Transfer 46 (2003) 949–961.
[16] S.I. Futko, Mechanism of upper temperature limits in a wave of filtration combustion of gases, Combust. Explosion Shock Waves 39 (2) (2003) 130–139.
[17] L.D. Mare, T.A. Mihalik, G. Continillo, J.H.S. Lee, Experimental and numerical study of flammability limits of gaseous mixtures in porous media, Exp. Therm. Fluid Sci. 21 (2000) 117–123.
[18] A.P. Aldushin, I.E. Rumanov, B.J. Matkowsky, Maximal energy accumulation in a superadiabatic filtration combustion wave, Combust. Flame 118 (1999) 76–90.
[19] G.E. Koester, Propagation of wave-like unstabilized combustion front in inert porous media, PhD Thesis, Department of Mechanical Engineering, The Ohio State University, Ohio, 1997.